NUMERICAL MODELING OF DAMAGE INITIATION AND FAILURE PROCESS IN POLYMER-CLAY NANOCOMPOSITES

Y. Chen[1], J.Y.H. Chia[1, 2], Z.C. Su[1], T.E. Tay[1], V.B.C. Tan[1, *]

[1]*Department of Mechanical Engineering, National University of Singapore, Singapore 117576*
[2]*Institute of Material Research and Engineering, A*STAR, 3 Research, Link, Singapore 117602*
**e-mail address: mpetanbc@nus.edu.sg*

Keywords: polymer-clay nanocomposites (PCNs), damage initiation, failure process, representative volume element (RVE).

Abstract
The damage initiation and failure process in polymer-clay nanocomposites (PCNs) are studied based on a representative volume element (RVE) model. The associated interfaces are modeled with cohesive zone model (CZM) and the matrix phase is modeled using material property degradation method (MPDM). Uni-axial tension is applied on the RVE model and periodic boundary conditions are maintained. Simulation results show that two sites of damage initiation - interlayer gallery and matrix phase - are identified. The former is more likely to occur due to the reduced stiffness and strength of the gallery because of void defects. Gallery damage occurs along with the formation of micro-cracks, which could gradually penetrate into the matrix phase and eventually develop into a complete fracture surface throughout the whole RVE model.

1 Introduction
Polymer-clay nanocomposites (PCNs) are found to exhibit unique and markedly improved material properties compared to pure matrix or traditional micro/macro composites. These superior properties include light weight, high mechanical performance, thermal stability, gas impermeability and flammability [1]. Despite the great potential of PCNs in engineering, the failure mechanisms of PCNs are not well understood. Some experimental techniques such as SEM and TEM have been utilized to investigate the failure process of PCNs [2-3]. However, these techniques can only examine material damage near the fracture surface but cannot identify the exact position of damage initiation and track the damage evolution dynamically. Furthermore, these techniques are limited in providing details about failure phenomena on the molecular level, such as the separation failure of nanosized interfaces and formation of nanosized cracks, because the equipment does not have the required resolution. It is expected that the numerical modeling could be an alternative to shed light on the failure mechanism of PCNs. This paper aims to develop a numerical approach for modeling the deformation and damage process of PCNs with main interests in identifying the damage initiation and evolution.

2 Model and progressive damage modeling
2.1 Representative volume element (RVE) model
The PCN consists of a polymer matrix and nanosized clay particles. Figure 1 shows its structure at different length scales. The PCN is usually treated as a typical multi-phase system

including the matrix phase, silicate sheets, gallery interfaces and interphase interfaces as labeled in Figure 1(b).

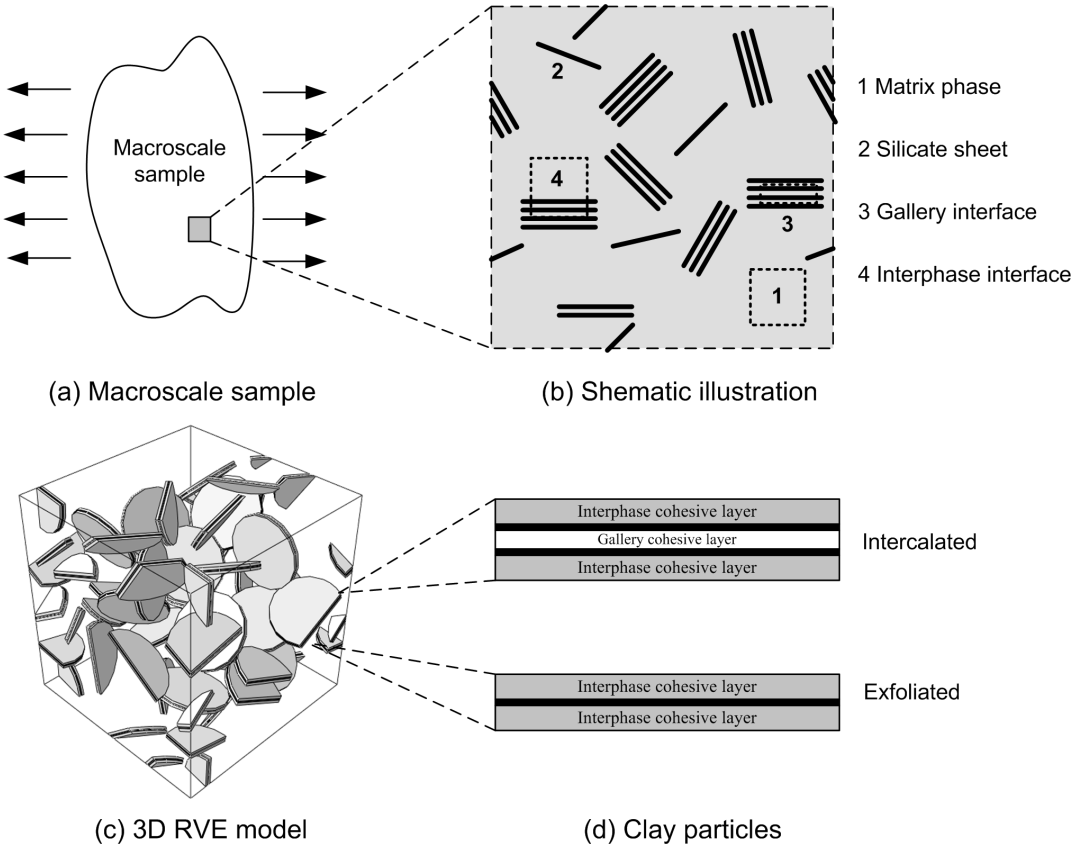

Figure 1. Polymer-clay nanocomposite at different length scales

Matrix phase: same polymer used in traditional composite materials and it is specified as a thermosetting epoxy system (DGEBA+DETDA) in this work.
Silicate sheet: the basic unit of clay particles. Fully exfoliated particles are in form of single silicate sheet while intercalated particles appear as stacked sheets. The silicate sheet has in-plane dimensions of 100-1000nm and a thickness of about 0.95nm.
Gallery interface: the organic interlayer between two stacked silicates sheets in intercalated clay particles. It only exists in intercalated sheets.
Interphase interface: the interfacial region between matrix phase and surface of the outside silicate sheet. It exists in both intercalated and exfoliated ones.

Figure 1 (c) shows a representative volume element (RVE) model of PCN. For intercalated particles with two stacked silicate sheets as an example, one gallery cohesive layer is sandwiched within silicate sheets and two interphase cohesive layers are positioned on two sides. For fully exfoliated ones in form of single silicate sheet, the gallery cohesive layer does not exist and only the interphase cohesive layers are modeled, as illustrated in Figure 1 (d).

2.2 Progressive damage modeling techniques
Both gallery and interphase interfaces are modeled using cohesive zone model with function to separate or split. A stress-based quadratic criterion is used for damage initiation and a tabular form of degradation is used for post damage evolution. The details can be found in [4].

The matrix phase is modeled using the material property degradation method (MPDM). This method assumes that the damaged materials can be replaced by an equivalent material with degraded stiffness. Once damage is detected, the MPDM is applied to the corresponding element. A modified version of von Mises failure criterion suggested by Christensen [5] is adopted as follows:

$$\frac{\sigma_{Mises}^2}{C_m T_m} + (\frac{1}{T_m} - \frac{1}{C_m}) I_1 = 1 \tag{1}$$

where T_m and C_m denote the tensile and compressive strength, σ_{Mises} and I_1 are von Mises equivalent stress and the first stress invariant of micro stresses, respectively. Once the damage criterion is satisfied, the elastic moduli of the element are modified. Internal state variables $d_i\,(i = 1,2...6)$ are used to fulfill the stiffness degradation of the failed elements. It is should be noted that the Poisson's ratios are not degraded, only the Young's and shear moduli are modified as follows:

$$\begin{aligned} &E_{11} = d_1 E_{11}^{\ 0} \quad E_{22} = d_2 E_{22}^{\ 0} \quad E_{33} = d_3 E_{33}^{\ 0} \\ &G_{12} = d_4 G_{12}^0 \quad G_{23} = d_5 G_{23}^0 \quad G_{13} = d_6 G_{13}^0 \end{aligned} \tag{2}$$

where $E_{11}, E_{22}, E_{33}, G_{12}, G_{23}, \text{and } G_{13}$ are the effective moduli of the damaged element, $E_{11}^0, E_{22}^0, E_{33}^0, G_{12}^0, G_{23}^0, \text{and } G_{13}^0$ are those of the undamaged element. As the matrix phase is treated as isotropic and elastic in this work, the six internal state variables d_i are set to be same and equal to 10^{-3} following the suggestion by Tabiei et al [6].

In order to present the stress intensity and damage situation in the matrix phase, a damage status variable (DSV) is introduced as follows:

$$\text{DSV} = \begin{cases} \dfrac{\sigma_{Mises}^2}{C_m T_m} + (\dfrac{1}{T_m} - \dfrac{1}{C_m}) I_1 & \text{before damage initiation} \\ 1 & \text{after damage initation} \end{cases} \tag{3}$$

The DSV value first increases with the applied strain and is smaller than 1. Once the failure criterion is satisfied, its value becomes 1, meaning the element is damaged and the value will keep constant in further loading. The DSV values are calculated for all matrix elements and the DSV contour will be used to present the stress intensity in critical regions and track how the damage evolves in the RVE model.

Table 1 shows the material properties of the constitutes of PCN. The tensile strength of epoxy matrix is taken as the maximum stress of its molecular model under uni-axial tension in molecular dynamics (MD) simulations [7]. The compressive strength is assumed to be same as the tensile strength. The moduli of cohesive layers are assumed to be same as the matrix phase. Their normal and shear cohesive strength are adopted as the peak strength of their traction-separation curves when subjected to a Mode I splitting in MD simulations [7]. For post damage evolution, the SDEG versus the separation distance is explicitly given in a tabular form.

Constituents	Material parameters	Values
Epoxy matrix	Young's modulus E (GPa)	3.2934
	Poisson's ratio ν	0.2867
	Tensile strength T_m (MPa)	153.74
	Compressive strength C_m (MPa)	153.74
Silicate sheet	Young's modulus E (Gpa)	430.9266
	Poisson's ratio ν	0.1459
Gallery cohesive layer	Cohesive layer thickness T_0 (nm)	2.0
	Cohesive modulus E_0 (Gpa)	3.2934
	Cohesive normal strength S_n (MPa)	99.87
	Cohesive shear strength $S_s = S_t$ (MPa)	99.87
Interphase cohesive layer	Cohesive layer thickness T_0 (nm)	6.0
	Cohesive modulus E_0 (Gpa)	3.2934
	Cohesive normal strength S_n (MPa)	131.07
	Cohesive shear strength $S_s = S_t$ (MPa)	131.07

Table 1. Material properties of the constituents of PCN.

3 Boundary condition

The RVE model is subjected to uni-axial tension. The periodicity of the RVE model during tension is maintained. Figure 2 shows the DSV contours of a RVE model with and without the periodic boundary condition (PBC). In the former case, it is obvious that the localized damaged band (red region) is forced to be follow periodicity and continuity when crossing the RVE boundary. Thus, the PBC is employed in further sections.

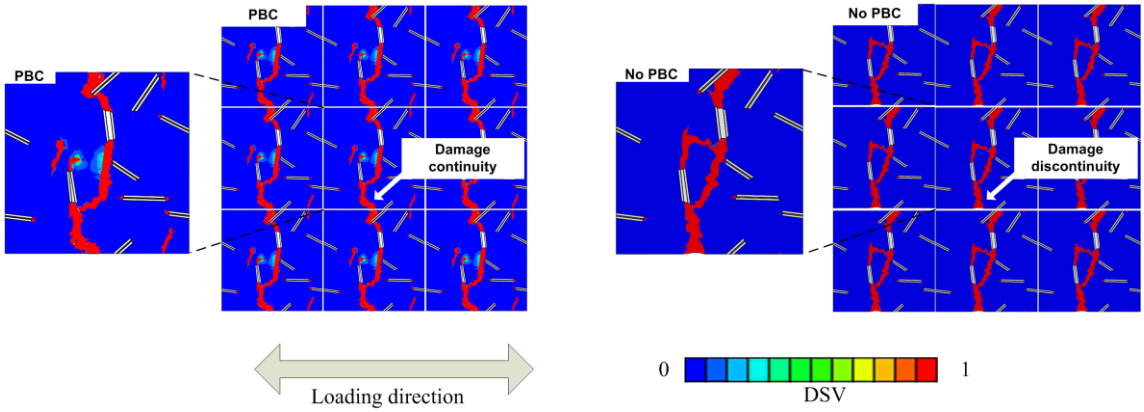

Figure 2. DSV contours of RVE model with and without periodic boundary condition.

4 Results and discussions

4.1 Damage initiation

For fully exfoliated particles in the form of single silicate sheets, epoxy molecules would easily cover the outside surfaces because of strong diffusion before the epoxy is cured. However, for intercalated particles, it is difficult for epoxy molecules to penetrate into the interlayer galleries whose thicknesses are only several nanometers. The nanosized gallery would lower the molecular mobility of epoxy molecules and hinder them from diffusing to the central regions of the galleries whose in-plane dimensions may be more than several hundred nm. Galleries that are not fully filled up with epoxy would have some local voids, which will inevitably lower its mechanical properties. In order to account for this, a defect factor k is introduced to scale the stiffness and peak strength of gallery cohesive layers. It should be pointed out that the failure separation distance δ is mainly controlled by the alkyl chain length of the surfactants [7] and therefore is not scaled. The fracture energy of the gallery cohesive layer will be correspondingly scaled down because of the decrease in peak strength.

Figure 3 shows the stress-strain curves of the RVE model containing intercalated particles with two silicate sheets stacked. Defect factors k ranging from 0.1 to 1 are examined. For all cases, the stress is linearly proportional to the tensile strain initially with the slope denoting Young's modulus. As the applied strain increases, the stress gradually becomes non-linear and before reaching a maximum value. It is apparent that the maximum stress is highly dependent on the defect factor k. More specifically, when k is higher or equal to 0.5, the stress-strain curves are the same and the maximum stresses are almost same. However, when k is lower than 0.5, the maximum stress becomes lower and is reached earlier. The lower the defect factor is, the lower the maximum stress is. In addition, the stress after the maximum value also exhibits different decreasing trends. The stress drop more quickly for higher defect factors k. It indicates that the defect factor k play an essential role in the micro-deformation process of PCN, which is responsible for the different stress-strain curves observed.

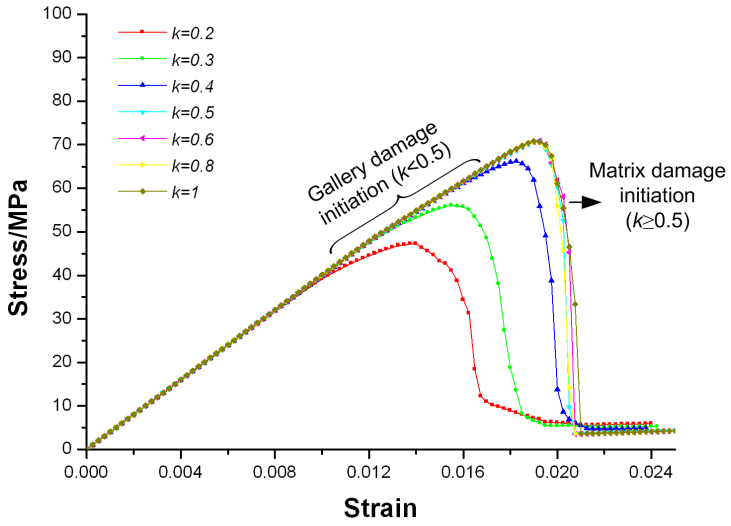

Figure 3. Stress-strain curves of RVE model with various defect factors.

Generally, the stress-strain curves can be divided into two catalogues according to the defect factor: (i) $k < 0.5$, (ii) $k \geq 0.5$. Here, two representative cases with $k = 0.4$ and 0.8 are selected for a comparative analysis.

Figure 4 plots the scalar damage variable (SDEG) of gallery and interphase interfaces as well as the stress-strain curve for the case of $k = 0.4$. The DSV contours of the matrix phase at critical stages are also shown. It is observed that the SDEG of gallery layer becomes non-zero when the strain reaches about 1.25%, indicating the occurrence of damage initiation in galleries along with the formation of interlayer micro-cracks. The micro-cracks gradually develop into the matrix phases when the strain increases to 1.825% as shown in the first DSV contour (long red arrow). With the extension of micro-cracks into the matrix, the high local stress around the gallery layer is released. Consequentially, the damage of gallery layer is gradually stopped as no increase in SDEG is observed. It is noted that these particles with damage initiation in gallery are more likely perpendicular to the loading direction as higher local stress concentration would appear in such particles. With further loading, the micro-cracks could merge together. They would also interact with other dispersed particles. Details will be presented in later sections.

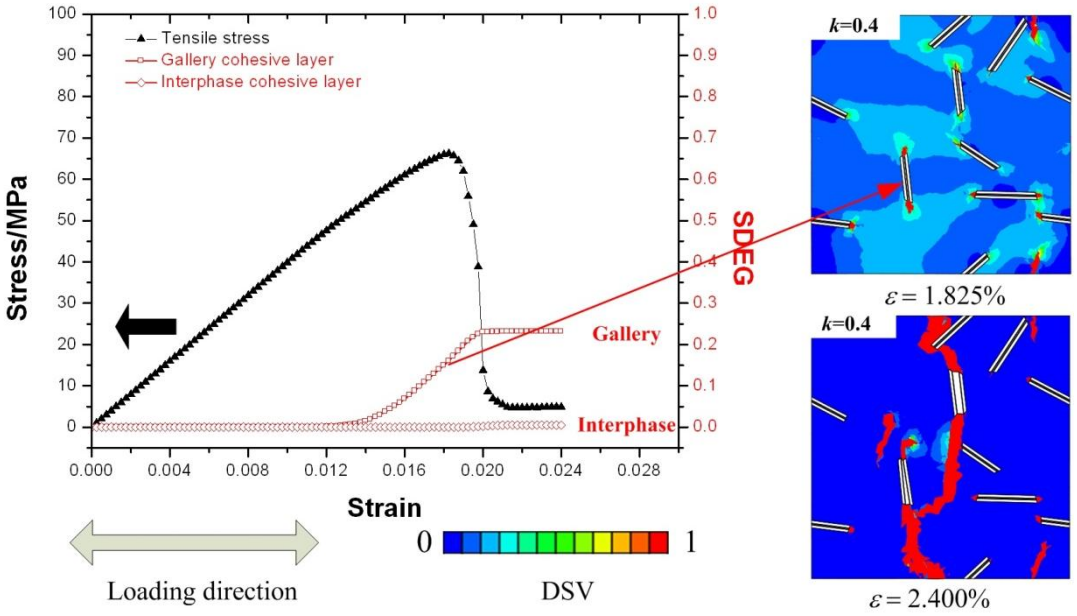

Figure 4. Stress-strain and SDEG curves as well as DSV contours of RVE model with defected factor k = 0.4.

Figure 5 shows the results of another simulation with k = 0.8. The SDEG of gallery cohesive layers remains zero, indicating no damage occurs within the gallery. This is also supported by the DSV contours, in which the fracture surface (red region) does not pass through any interlayer gallery. The damage initiation occurs in the matrix phase in the vicinity of particles instead of within the gallery. After that, the damage in the matrix would develop throughout the whole RVE domain with further loading.

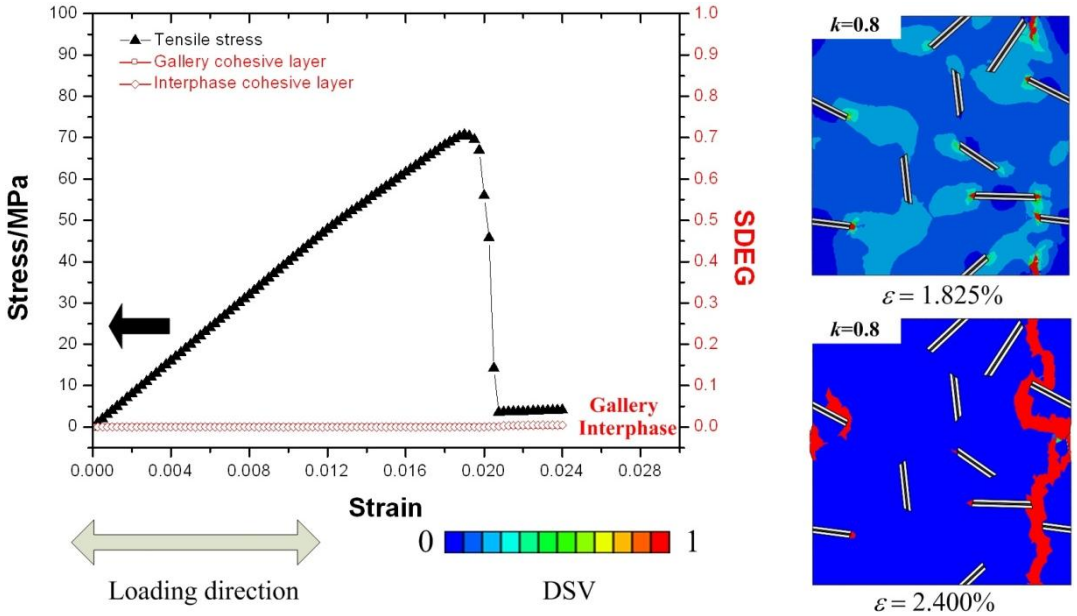

Figure 5. Stress-strain and SDEG curves as well as DSV contours of RVE model with defected factor k = 0.8.

It is apparent that two different patterns of damage initiation are identified. The first type is the damage initiation in the gallery along with formation of micro-cracks. The second type is the damage initiation in the matrix phase around the tip of particles and this type would occur if only the gallery strength is high enough and the matrix damage criterion is satisfied first. It is clear that the occurrence of damage initiation is dominated by the stiffness and strength of

the interlayer gallery, which are determined by the interlayer molecular structure. In actual materials, particles with defective galleries inevitably exist and they would act as damage initiator and nucleation of micro-cracks. It has been confirmed by several experimental studies that micro-cracks resulting from gallery damage are observed in both thermoplastic [3] and thermosetting [2] based nanocomposites. Figure 6 shows a TEM observation of such micro-cracks (also called micro-voids) formed within stacked particles. Wang et al [2] pointed out that that such micro-crack characterizes most damage initiation in nanocomposites. Kim and co-works [3] also observed such phenomenon and believed that the weak bonding between silicate sheets was responsible for the nucleation of micro-cracks. Essentially, the weak debonding between silicate sheets by Kim is identical to the lowed stiffness and strength of the gallery cohesive layer resulting from defective molecular structure as suggested in this work.

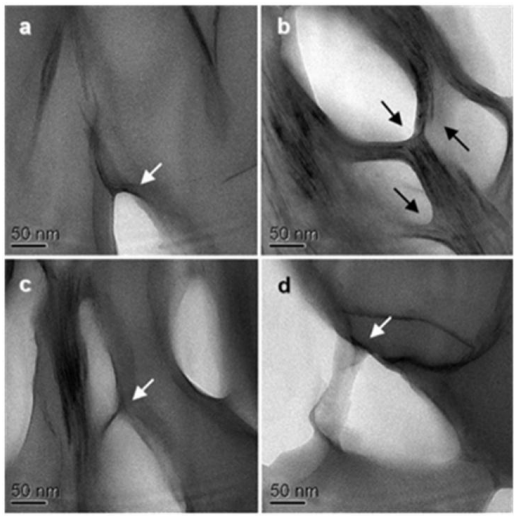

Figure 6. TEM micrographs of micro-cracks resulting from gallery damage [2].

4.2 Failure Process

This section will discuss how the damage evolves in the RVE model, i.e, crack propagation, especially how it interacts with dispersed particles when they meet. Figure 7 shows the DSV contours from two sectional views normal to the loading direction, mimicking TEM observations. Basically, there are two main ways for the crack to propagate when its tip meets the clay particle: (i) it may penetrate into one gallery of the stacked particle, split the particle and continue propagating if the clay particle is oriented almost parallel to the propagating crack, or (ii) it may be deflected to the outside surface if the clay particle is not parallel to the crack. Essentially, whether the cracks are able to split a stacked particle or be deflected by the particle depends on its orientation.

The two propagating paths have also been observed and confirmed in experiments [2]. Wang showed a stable crack propagation path traced by TEM in Figure 7. The crack tip reaches site A first (Figure 7 a) where the clay particle is almost perpendicular to the crack. Evidently, the clay particle hinders crack propagation. Although some micro-cracks nucleated in front of the main crack (below site A), the rigid clay particle do not break and give way to allow crack propagation. As a result, the crack deflects and extends along the outside surface the particle. When the crack meets a particle that is almost parallel to the crack propagation direction, like site B, the crack could proceed ahead by splitting the stacked particle, breaking matrix ligaments and merging with other micro-cracks.

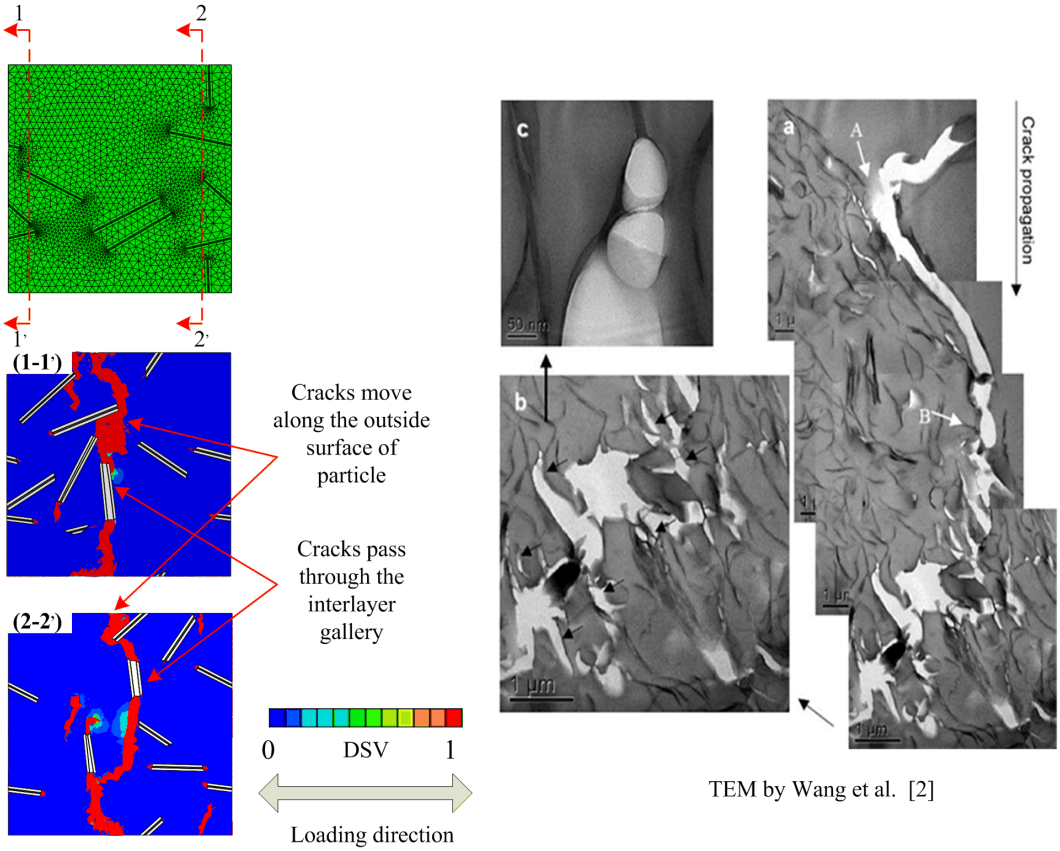

Figure 7. Crack propagation in RVE model.

5 Conclusions

This paper demonstrates a finite element RVE based numerical approach for investigating the damage initiation and failure process in PCNs. This study is a starting point for using continuum modeling methods to elucidate the complex failure mechanisms of PCNs. Further research will focus on bridging the micro-deformation processes with the mechanical behavior of PCNs, including their tensile strength and fracture toughness.

References

[1] Alexander M., Dubois P., Polymer-layered silicate nanocomposites: preparation, properties and uses of a new class of materials, *Materials Science and Engineering: R: Reports*, 28, pp.1-63 (2000).

[2] Wang K., Chen L., Wu J.S., Toh M. L., He C.B. and Yee A. F., Epoxy nanocomposites with highly exfoliated clay: mechanical properties and fracture mechanisms, *Macromolecules*, 38, pp.788-800 (2005).

[3] Kim G.M., Lee D. H., Hoffmann B., Kressler J., Stoppelmann G., Influence of nanofillers on the deformation process in layered silicate/polyamide-12 nanocomposites, *Polymer*, 42, pp.1095-1100 (2001).

[4] ABAQUS version 6.10, SIMULIA, Dassault System.

[5] Christensen R.M, A comprehensive theory of yielding and failure for isotropic materials, *Journal of Engineering Materials and Technology*, 129, pp.173-181 (2007).

[6] Tabiei A., Ivanov I., Materially and geometrically non-linear woven composites micro-mechanical model with failure for finite element simulations, *International Journal of Non-Linear Mechanics*, 39, pp.175-188 (2004).

[7] Chen Y., Multisclae modeling approach of polymer-clay nanocoposites, PhD thesis in preparation (2012).